

# Impact of the vector interaction on the phase structure of QCD matter

A. V. Friesen,<sup>1</sup> Yu. L. Kalinovsky,<sup>1</sup> and V. D. Toneev<sup>1</sup>

<sup>1</sup>*Joint Institute for Nuclear Research, Dubna, Russia*

The 2-flavor Polyakov-loop extended model is generalized by taking into account the effective four-quark vector-type interaction with the coupling strengths, which are endowed with a dependence on the Polyakov field  $\Phi$ . The effective vertex generates entanglement interaction between the Polyakov loop and the chiral condensate. We investigate the influence of an additional quark vector interaction and the entanglement interaction on the location of the critical end-point at the given chemical potential or quark density. It is shown that the finite value of the vector interaction strength  $G_v$  improves the model agreement with the lattice data. The influence of the non-zero  $G_v$  and entanglement on the thermodynamic observables and the curvature of the crossover boundary in the  $T - \mu$  plane is also examined.

PACS numbers: 11.30.Rd, 12.20.Ds, 14.40.Be  
Keywords:

## I. INTRODUCTION

The QCD phase diagram and transitions between quark and hadron phases are in the focus of recent investigations in both theoretical and experimental fields of heavy energy physics. However, investigation of the matter at finite temperature and real chemical potential is difficult. Although the lattice theory has made progress last years in calculations at the finite chemical potential, the effective models are still most useful, for example, Nambu-Jona-Lasinio-like models.

On the basis of the NJL model it is possible to build a phase diagram describing the chiral restoration phase transition. There are a crossover phase transition at low and intermediate  $\mu$  and the first order transition at large  $\mu$ . The NJL model can describe chiral symmetry breaking, but not the confinement mechanism. The PNJL model is designed [1] to make it possible to treat both the mechanisms. To describe the quark-gluon coupling and confinement transition, the Polyakov loop has to be included. The PNJL model can reproduce results of lattice QCD at zero and imaginary  $\mu$ , where LQCD has no sign problem. However, the PNJL and lattice results for calculation of chiral transition temperature at  $\mu = 0$  do not coincide. Then it was suggested renormalizing the lattice transition temperature for pure gluon system  $T_0 = 0.27$  GeV as  $T_0 = 0.19$  GeV to get a realistic transition temperature ( $T_c^{\text{lat}} \sim 0.16 - 0.19$  GeV) [2]. It leads to a divergence of the chiral transition and deconfinement transition temperatures at the zero chemical potential in PNJL which do not coincide with the lattice results too. To improve this situation, it was suggested that strong correlations (entanglement) between the chiral and deconfinement crossover transitions should be introduced by including an additional dependence of the four-quark interaction on the Polyakov loop [3, 4]. The model was called later the entanglement-PNJL (EPNJL) model.

In the PNJL model, the correlation between quark and gauge fields is weak, so that the chiral and deconfinement crossover transitions do not coincide without any fine-tuning of parameters [5]. For the zero chemical poten-

tial, the scalar type eight-quark interaction is necessary to obtain a coincidence between the two transitions, or the vector-type four-quark interaction is needed [5]. This fact indicates that a true correlation between the quark condensate and the Polyakov loop is stronger than that in the standard PNJL model appearing through the covariant derivative between quark and gauge fields. The problem of the existence of the critical end point and first order transition on the phase diagram is still under consideration. The inclusion of the vector interaction in the NJL or PNJL models was discussed, for example in [6–8]. In Refs. [5, 9], it was shown that the equation of state depends on the vector coupling constant  $G_v$ . When the vector interaction is taken into account, the first order transition area becomes smaller, the critical point appears at a higher chemical potential and lower temperature and is even capable of removing the first order phase transition completely from the phase diagram.

This paper studies the effects of the inclusion of the vector quark interaction and its entanglement with the Polyakov loop, their interplay as well as their influence on the thermodynamic behavior of a quark system.

## II. PNJL WITH VECTOR INTERACTION

We use the standard PNJL Lagrangian with the vector interaction term

$$\begin{aligned} \mathcal{L}_{\text{PNJL}} = & \bar{q} (i\gamma_\mu D^\mu - \hat{m}_0) q + G_s \left[ (\bar{q}q)^2 + (\bar{q}i\gamma_5 \vec{\tau}q)^2 \right] \\ & - G_v (\bar{q}\gamma_\mu q)^2 - \mathcal{U}(\Phi[A], \bar{\Phi}[A]; T) . \end{aligned} \quad (1)$$

A local chirally symmetric scalar-pseudoscalar four-point interaction of quark fields  $q, \bar{q}$  is introduced with an effective coupling strength  $G_s$ , and the vector interaction strength is regulated by  $G_v$ ;  $\vec{\tau}$  is the vector of the Pauli matrices in flavor space,  $\hat{m}_0$  is the diagonal matrix of the 2-flavor current quark masses  $m_u^0 = m_d^0 = m_0$ . The quark fields are coupled to the gauge field  $A^\mu$  through the covariant derivative

$$D^\mu = \partial^\mu - iA^\mu. \quad (2)$$

The gauge coupling  $g$  is conveniently absorbed in the definition  $A^\mu(x) = g\mathcal{A}_a^\mu \frac{\lambda_a}{2}$  where  $\mathcal{A}_a^\mu$  is the  $SU(3)$  gauge field and  $\lambda_a$  is the Gell-Mann matrices. The gauge field is taken in the Polyakov gauge  $A^\mu = \delta_0^\mu A^0 = -i\delta_4^\mu A_4$ . The field  $\Phi$  is determined by the trace of the Polyakov loop  $L(\vec{x})$  and its conjugate

$$\begin{aligned}\Phi[A] &= \frac{1}{N_c} \text{Tr}_c L(\vec{x}) \\ &= \frac{1}{N_c} \text{Tr}_c \left\{ \mathcal{P} \exp \left[ i \int_0^\beta d\tau A_4(\vec{x}, \tau) \right] \right\}\end{aligned}\quad (3)$$

with  $\beta = 1/T$  being the inverse temperature and  $\mathcal{P}$  being the path ordering. In the absence of quarks, we have  $\Phi = \bar{\Phi}$  and the Polyakov loop serves as an order parameter for deconfinement. The Polyakov loop  $\Phi$  is an exact order parameter of spontaneous  $Z_3$  symmetry breaking in pure gauge theory. Although  $Z_3$  symmetry is not exact in the system with dynamical quarks, it still seems to be a good indicator of the deconfinement phase transition. Therefore, we use  $\Phi$  to define the deconfinement phase transition.

An effective potential  $\mathcal{U}(\Phi[A], \bar{\Phi}[A]; T)$  describes the gauge sector and must satisfy the  $Z(3)$  center symmetry; therefore, one can choose any form satisfying the symmetry conditions [10], but in this work the following general polynomial form with the same parameters is used [2]:

$$\begin{aligned}\frac{\mathcal{U}(\Phi, \bar{\Phi}; T)}{T^4} &= -\frac{b_2(T)}{2} \bar{\Phi}\Phi - \frac{b_3}{6} (\Phi^3 + \bar{\Phi}^3) + \frac{b_4}{4} (\bar{\Phi}\Phi)^2 \\ b_2(T) &= a_0 + a_1 \left(\frac{T_0}{T}\right) + a_2 \left(\frac{T_0}{T}\right)^2 + a_3 \left(\frac{T_0}{T}\right)^3.\end{aligned}\quad (4)$$

$T_0 = 0.27$  GeV is the critical temperature of the deconfinement transition in the pure gauge limit when quarks are assumed to be infinitely heavy.

The grand potential density for the PNJL ( $N_f = 2$ ) model in the mean-field approximation can be obtained from the Lagrangian density (1) as [2, 11]:

$$\Omega(\Phi, \bar{\Phi}, m, T, \mu) = \mathcal{U}(\Phi, \bar{\Phi}; T) + G_s \sigma^2 + G_v \rho^2 + \Omega_q \quad (5)$$

where  $\sigma = \langle \bar{q}q \rangle$  is the quark condensate,  $\rho = \langle \bar{q}\gamma_0 q \rangle$  is the quark density and the quark term is

$$\begin{aligned}\Omega_q &= -2N_c N_f \int \frac{d^3p}{(2\pi)^3} E_p \\ &\quad - 2N_f T \int \frac{d^3p}{(2\pi)^3} \left[ \ln N_\Phi^+(E_p) + \ln N_\Phi^-(E_p) \right]\end{aligned}\quad (6)$$

with the functions

$$N_\Phi^+ = \left[ 1 + 3 \left( \Phi + \bar{\Phi} e^{-\beta E_p^+} \right) e^{-\beta E_p^+} + e^{-3\beta E_p^+} \right], \quad (7)$$

$$N_\Phi^- = \left[ 1 + 3 \left( \bar{\Phi} + \Phi e^{-\beta E_p^-} \right) e^{-\beta E_p^-} + e^{-3\beta E_p^-} \right] \quad (8)$$

where  $E_p = \sqrt{\mathbf{p}^2 + m^2}$  is the quasiparticle energy of the quark;  $E_p^\pm = E_p \mp \tilde{\mu}$  and  $\tilde{\mu}$  is related with the quark chemical potential  $\mu$  and the quark density through  $G_v$ .

After performing the hadronization procedure the constituent quark mass  $m$  can be obtained as a solution of the gap equation (by minimization of  $\Omega$  with respect to  $m$ :  $\partial\Omega/\partial m = 0$ ). This condition is equivalent to the gap equation [2, 11]. There is also an equation for  $\tilde{\mu}$  obtained as  $\partial\Omega/\partial\rho = 0$ .

$$m = m_0 - 2G_s \sigma, \quad (9)$$

$$\tilde{\mu} = \mu - 2G_v \rho. \quad (10)$$

Moreover, for PNJL calculations we should find values of  $\Phi$  and  $\bar{\Phi}$  by minimizing  $\Omega$  with respect to  $\Phi$  and  $\bar{\Phi}$  [11] at given  $T$  and  $\mu$ .

For the mass gap equation we get

$$m = m_0 + 4G_s N_c N_f \int_\Lambda \frac{d^3p}{(2\pi)^3} \frac{m}{E_p} [1 - f^+ - f^-] \quad (11)$$

and for  $\tilde{\mu}$

$$\tilde{\mu} = \mu - 4G_v N_c N_f \int_\Lambda \frac{d^3p}{(2\pi)^3} \frac{m}{E_p} [f^+ - f^-] \quad (12)$$

with the modified Fermi-Dirac distribution functions for fermions and antifermions

$$f^+ = \left[ \left( \Phi + 2\bar{\Phi} e^{-\beta E_p^+} \right) e^{-\beta E_p^+} + e^{-3\beta E_p^+} \right] / N_\Phi^+, \quad (13)$$

$$f^- = \left[ \left( \bar{\Phi} + 2\Phi e^{-\beta E_p^-} \right) e^{-\beta E_p^-} + e^{-3\beta E_p^-} \right] / N_\Phi^-. \quad (14)$$

One should note that if  $\Phi \rightarrow 1$ , Eqs. (13),(14) reduce to the standard NJL model.

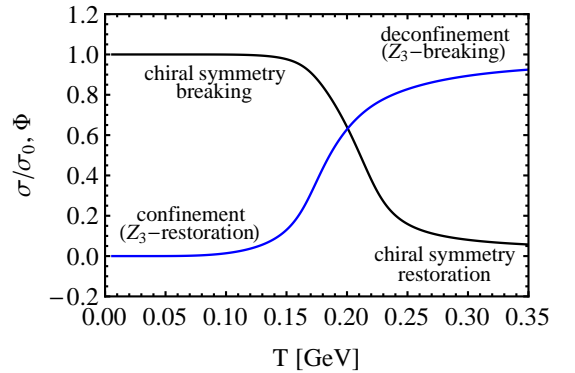


FIG. 1: Condensate normalized to  $\sigma_0 = \sigma(T = 0, \mu = 0)$  and the Polyakov loop as order parameters for the chiral phase transitions and confinement, respectively.

To obtain free parameters in NJL-like models, the vacuum values of  $m_\pi = 0.139$ ,  $\sigma^{1/3} = -0.25$  GeV and  $f_\pi = 0.092$  should be reproduced. In this work, the parameters  $\Lambda = 0.639$  GeV,  $m_0 = 0.0055$  GeV and  $G_s = 5.227$  GeV<sup>-2</sup> and the same parameters for the effective potential as in [2, 11] are used. The parameter  $T_0$  is renormalized to  $T_0 = 0.19$  GeV to make the critical temperature lower (see [2, 11]).

From a theoretical point of view the QCD phase diagram on the  $(\mu, T)$ -plane has the following structure: there are a hadron phase of confined quarks and gluons and the quark-gluon phase where deconfinement takes place. Both these phases are separated by a crossover transition at low density or chemical potential and temperature  $\sim 0.17$  GeV. When the chemical potential reaches a critical value, the crossover turns into the first order transition. At the turning point named the critical end point the second order transition takes place.

The  $Z_3$ -symmetry is explicitly broken in the presence of quarks with the noninfinite mass and non-vanishing Polyakov loop. Really, the phase structure of the quark models under discussion is determined by the behavior of the order parameters  $\sigma$ ,  $\Phi$  and  $\bar{\Phi}$  as a function of temperature and quark chemical potential. In the  $\mu = 0$  case it is illustrated in Fig. 1. The Polyakov loop  $\Phi$  vanishes at low temperature where the confinement takes place. At the same time, the chiral symmetry is explicitly broken by non-zero quark mass (at low temperatures). Confinement implies spontaneous brake of the chiral symmetry. Are the spontaneous brake of chiral symmetry imply confinement? Do they connected? Lattice QCD computations with 2+1 flavors gave the chiral transition temperature  $T_c^{\text{lat}} \sim 0.19$  GeV [12] (or 0.160 GeV in more recent computations [13, 14]). Pure gauge QCD on the lattice without quarks gives the first order deconfinement transition at  $T_0 = 0.27$  GeV. When the light quarks are added,  $Z_3$  symmetry is implicitly broken and deconfinement transition takes place at  $\sim 0.2$  GeV.

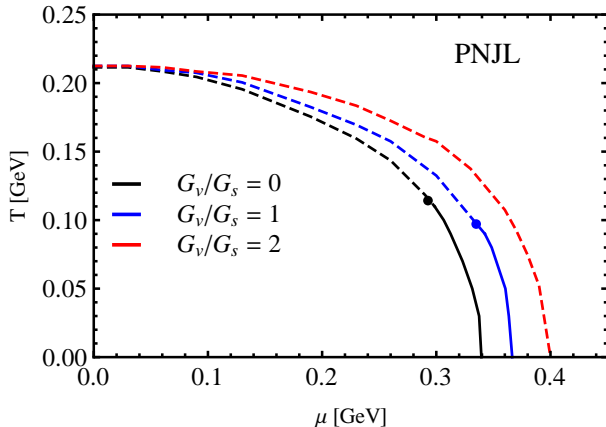


FIG. 2: Phase diagram of the PNJL model with vector interaction for the fixed ratio  $G_v/G_s$ .

As noted above, the order parameter of the spontaneous chiral symmetry is the quark condensate  $\sigma$ . In the Wigner-Weyl realization the condensate "melts" and disappears above a characteristic transition temperature. In the NJL and PNJL models the crossover transition temperature is indicated as a maximum of  $\frac{\partial\sigma}{\partial T}$  for each  $\mu$ . The first order phase transition is defined as  $\max \frac{\partial\rho}{\partial\mu}$  for

each  $T$ .

The inclusion of the vector interaction in the NJL or PNJL models discussed, for example in [5–7, 9], leads to the dependence of the equation of state on the vector coupling constant  $G_v$ . The first order transition area becomes smaller and the critical point appears at higher chemical potential and at lower temperature. In Fig. 2, the phase diagram of hadron matter is shown for the PNJL model with vector interaction at different values of  $G_v/G_s$ . The case  $G_v/G_s = 0$  displays a familiar picture of the chiral crossover terminating as a second order transition at a critical point. It was obtained that if the vector coupling  $G_v/G_s > 1.5$ , the first order transition region disappears completely and there exists a crossover transition only.

### III. ENTANGLEMENT OF DECONFINEMENT AND CHIRAL SYMMETRY

One of the problems of the phase diagram construction is the so-called pseudo-critical temperature  $T_c$  definition at the low chemical potential. Lattice calculations defined that  $T_c^{\text{lat}} = 0.173 \pm 8$  GeV; however  $T_c$  from NJL calculation is higher. Particularly, in the PNJL model  $T_c$  depends on the parameter of the effective potential  $T_0 = 0.27$  GeV (see Eq. (4)). When  $T_0$  is renormalized to reach agreement with lattice results, the chiral phase transition and deconfinement transition take place at different temperatures, while the lattice results show

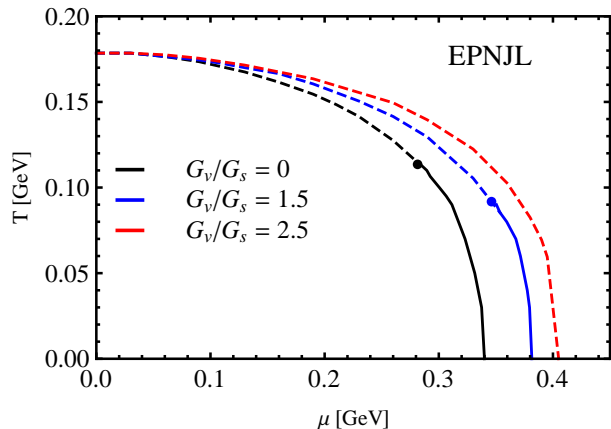


FIG. 3: Phase diagram of the EPNJL model with vector interaction for the fixed ratio  $\tilde{G}_v/\tilde{G}_s$ .

their coincidence. In [2, 11], it was suggested to define the pseudo-critical temperature as  $T_c = \frac{T_\sigma + T_\Phi}{2}$ , where  $T_\sigma = \frac{\partial\sigma}{\partial T}$  is the chiral transition temperature and  $T_\Phi = \frac{\partial\Phi}{\partial T}$  is the deconfinement transition temperature. However, it does not lead to the improvement of the situation with the difference between the crossover and

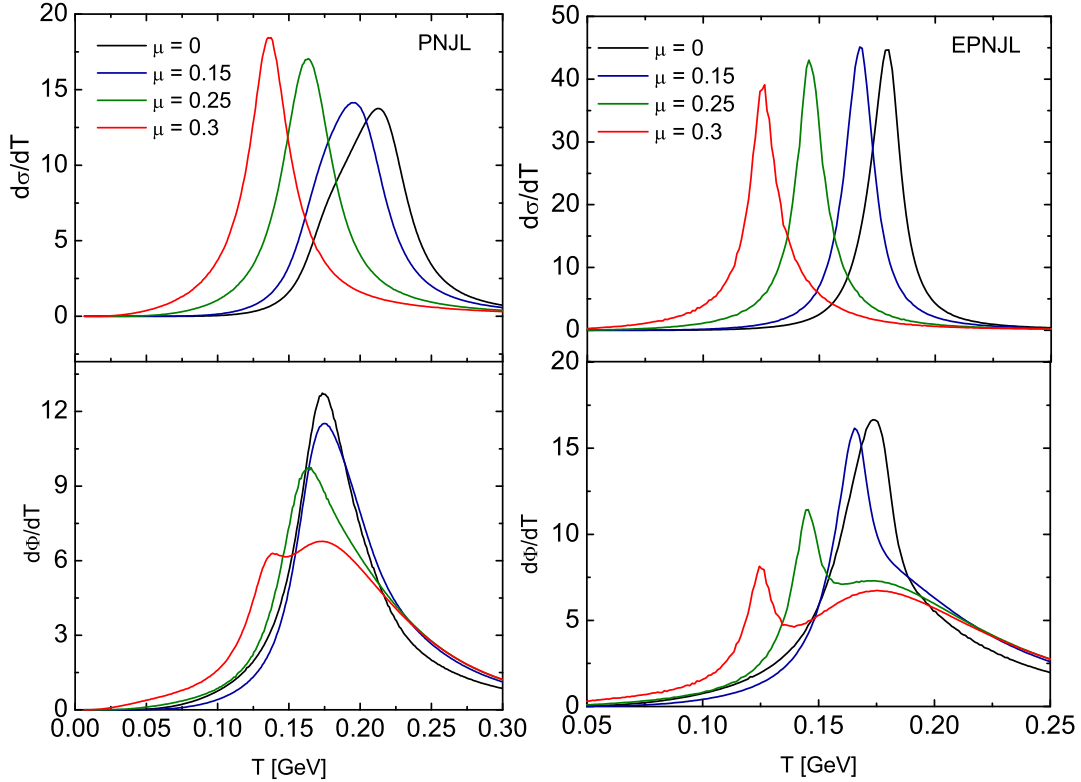


FIG. 4: Temperature dependence of the order parameters for various chemical potentials in the PNJL (left panel) and the EPNJL model (right panel) with the vector interaction for  $\tilde{G}_v/\tilde{G}_s = 1.5$ .

deconfinement temperatures, because the entanglement between the chiral and deconfinement transitions given only by Eq. (2) is weak. As it has been explained above, LQCD has the "sign" problem in calculation at finite  $\mu$ . One of the approaches to solve the problem is the introduction of the imaginary chemical potential [15–19]. Following the lattice imaginary potential in [5, 20] the imaginary chemical potential was introduced for vector-type four-quark and eight-quark interactions in Refs. [5, 9]. Later it was suggested that there should exist entanglement between chiral and deconfinement transition [3]. So the renormalized scalar and vector four-quark couplings were introduced as

$$\tilde{G}_s(\Phi) = G_s[1 - \alpha_1\Phi\bar{\Phi} - \alpha_2(\Phi^3 + \bar{\Phi}^3)], \quad (15)$$

where the parameters  $\alpha_1 = \alpha_2 = 0.2$  and  $T_0 = 0.19$  GeV are chosen to reproduce the LQCD data for  $\mu = 0$  [15]. In Refs. [21, 22], the entanglement as Eq. (15) is used for a real chemical potential. Following [23], the vector interaction coupling constant can be introduced as

$$\tilde{G}_v(\Phi) = G_v[1 - \alpha_1\Phi\bar{\Phi} - \alpha_2(\Phi^3 + \bar{\Phi}^3)] \quad (16)$$

and therefore the scalar and vector couplings  $\tilde{G}_v$  and  $\tilde{G}_s$  become temperature-dependent in this model. To keep

the ratio  $\tilde{G}_v/\tilde{G}_s$  independent of  $\Phi$ , we use the same  $\alpha_1, \alpha_2$  as for  $\tilde{G}_s$ .

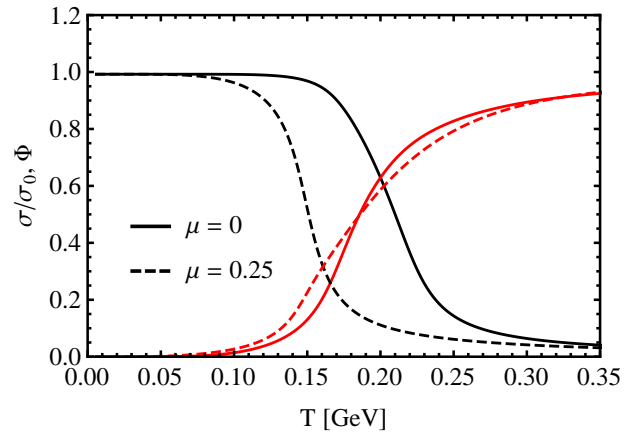


FIG. 5: The normalized condensate and Polyakov loop for the PNJL model at two different chemical potentials.

The phase diagram for the EPNJL model is shown in Fig. 3. Similarly to the case of the PNJL model (Fig. 2) the modified vector interaction splits the phase curves  $T - \mu$  and this splitting is the larger the vector

coupling. In the case of the EPNJL model the critical temperature at  $\mu = 0$  turns out to be the same as in the lattice calculations, and the appropriate critical end-points are situated at higher temperature than in the PNJL case.

The order parameters for both models are presented in Fig. 4. It is clearly seen that in the PNJL model the locations of maxima defined as temperature derivatives of  $\sigma$  and  $\Phi$  (compare the upper and bottom panels in the left column) are very different at low  $\mu$  and therefore the critical chiral and deconfinement temperatures are far from coincidence. The reason for that is the renormalization of  $T_0$ . However, if entanglement is taken into account, the peak positions coincide even at low  $\mu$  (see the right panel in Fig. 4). Moreover, in this case without entanglement one can observe from Fig. 4 (left bottom panel) that the derivative  $\partial\Phi/\partial T$  has two peaks at chemical potential near the critical value. The existence of two peaks can be related to coupling between the equations  $\partial\Omega/\partial m = 0$  and  $\partial\Omega/\partial\Phi = 0$  (see Fig. 5 for comparison). The first peak in  $\partial\Phi/\partial T$  is associated with the deconfinement transition and comes from the abrupt fall in the quark condensate  $\sigma$ . It is related to the Polyakov loop and its temperature coincides with the chiral transition temperature. The second peak arises from the Polyakov loop dynamics itself [10, 24].

It can be seen that at the zero chemical potential the areas of falling are closer to each other (solid lines), but at the high chemical potential the falling of quark condensate takes place earlier than for the Polyakov loop (dashed lines), which leads to arising of two peaks.

#### IV. COMPARISON WITH LATTICE QCD AND THERMODYNAMICS OF MODELS

The investigation of thermodynamics of a system starts with the grand canonical ensemble, which is related to the Hamiltonian  $H$  as follows:

$$e^{-\beta V\Omega} = \text{Tr} e^{-\beta(H-\mu N)}, \quad (17)$$

where  $N$  is the particle number operator,  $\mu$  is the quark chemical potential and the operator  $\text{Tr}$  is taken over momenta as well as color, flavor and Dirac indices. The considered models have the thermodynamic potentials defined from Eq. (5). It has the vacuum part that does not vanish as  $T \rightarrow 0$  and  $\mu \rightarrow 0$

$$\Omega_{vac} = \frac{(m - m_0)^2}{4G} - 2N_c N_f \int \frac{d^3p}{(2\pi)^3} E_p. \quad (18)$$

Basic thermodynamic quantities such as the pressure  $P$ , energy density  $\varepsilon$ , entropy density  $s$ , density of quark number  $\rho$  and the specific heat  $C_V$  - can be defined from

Eq.(17) as:

$$P = -\frac{\Omega}{V}, \quad (19)$$

$$s = -\left(\frac{\partial\Omega}{\partial T}\right)_\mu, \quad (20)$$

$$\varepsilon = -P + Ts + \mu\rho, \quad (21)$$

$$\rho = -\left(\frac{\partial\Omega}{\partial\mu}\right)_T, \quad (22)$$

$$C_V = \frac{T}{V} \left(\frac{\partial s}{\partial T}\right)_V. \quad (23)$$

In order to obtain the physical thermodynamic potential, which corresponds to vanishing pressure and energy density at  $(T, \mu) = (0, 0)$ , one has to renormalize the thermodynamic potential by subtracting its vacuum expression, Eq. (18). This corresponds to the following definition of the physical pressure:

$$\frac{\Delta P}{T^4} = \frac{P(T, \mu, m) - P(0, 0, m)}{T^4}. \quad (24)$$

In Fig. 6, the reduced pressure for both models is shown as a function of temperature at various  $G_v$ . The lattice results are taken from [27, 28] for the zero chemical potential. As is seen, at the zero chemical potential the results for  $G_v(\tilde{G}_v) = 0$  and  $G_v(\tilde{G}_v) \neq 0$  just coincide since there is no  $n_q$  in Eq. 19. In contrast, the normalized quark density is quite sensitive to the vector coupling. The dependence of quark density on the chemical potential  $\mu$  and the vector coupling  $G_v$  is shown in Fig. 7. The presented results clearly demonstrate that for agreement with the LQCD the vector coupling  $G_v$  should be finite and grow with  $\mu$  reaching approximately  $0.5G_s$  and  $1.5G_s$  in the PNJL and EPNJL models, respectively. The strength of  $G_v$  was estimated in Ref. [20] from the 2-flavor LQCD results for the deconfinement transition line at the imaginary chemical potential within the PNJL model including scalar eight-quark interaction in addition to the vector and scalar four-quark interactions. They suggested that  $G_v/G_s \approx 0.8$  in this model. A similar analysis based on the non-local PNJL model gives  $G_v/G_s \approx 0.4$  [29]. Recently, it was concluded within the 3-flavor PNJL model that  $G_v$  is nearly zero [30]. In the  $G_v$  estimates mentioned [20, 29, 30], the entanglement effect is not considered.

The temperature behavior of the order parameters, quark condensate  $\sigma$  and the Polyakov loop  $\Phi$  is compared to the lattice data in Fig. 8. Both models qualitatively reproduce the lattice experiment, but the agreement with lattice is better for the EPNJL description.

As has been noted above, in finite chemical potential calculations there exists "sign" problem in Lattice QCD. However, the introduction of the imaginary chemical potential allows one to solve the problem. In Ref. [31], it is suggested that the critical end-point be searched as a common point where the phase transition lines for all observables (the Polyakov loop, the strange quark number susceptibility, the chiral condensate and the chiral

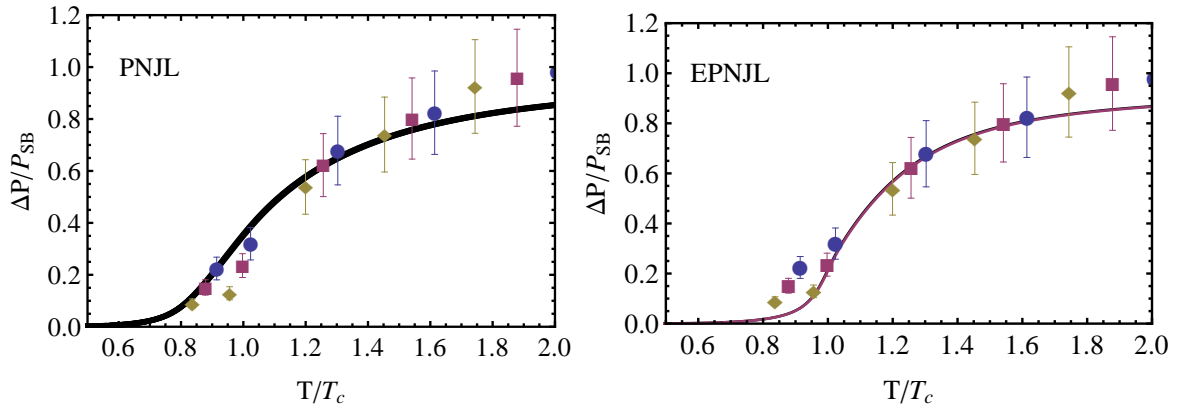


FIG. 6: Comparison of the normalized pressure with the lattice results for PNJL and EPNJL models at  $\mu = 0$  GeV. In both models the pressure is calculated for  $G_v = 0$  and  $G_v = 2G_s$ . In the EPNJL case both lines coincide. Lattice results are from [25]

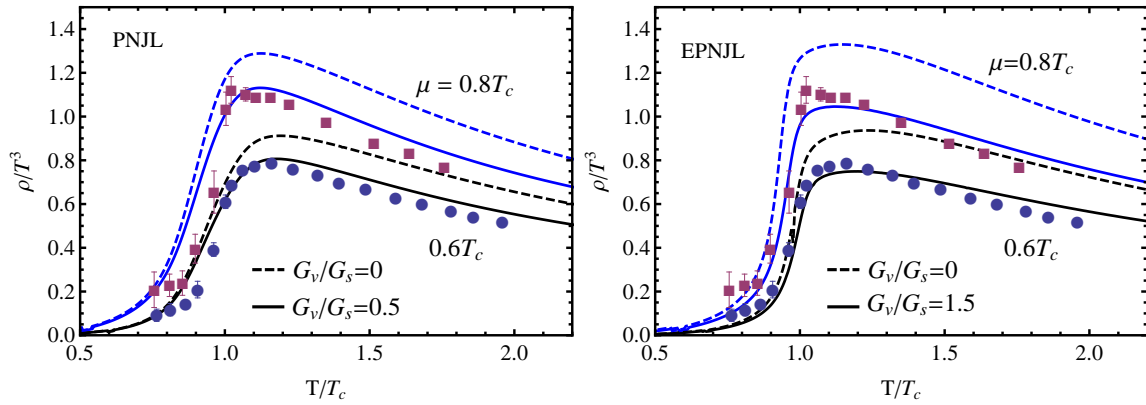


FIG. 7: Comparison between the lattice results [26] and the PNJL/EPNJL models for the normalized quark density at  $\mu = 0.6$  and  $0.8$  GeV.

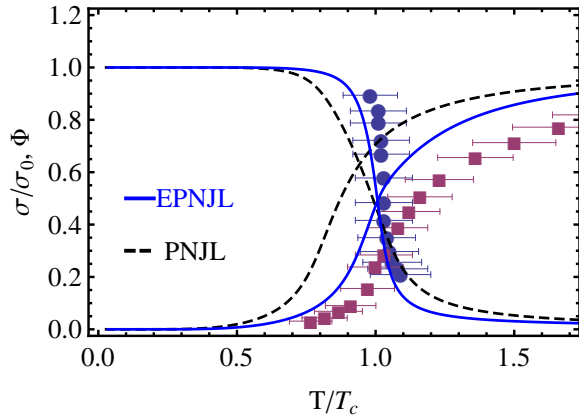


FIG. 8: Comparison of the normalized chiral condensate and Polyakov loop with the lattice results [28] at  $\mu = 0$  and  $G_v = 0$ .

susceptibility) converge. The simplest parameter of convergence is the curvature of the transition line

$$\frac{T_c(\mu)}{T_c(0)} = 1 - k \left( \frac{\mu}{T_c(\mu)} \right)^2. \quad (25)$$

The curvature  $k$  can be obtained in lattice QCD simulations in various ways by suitable combinations of ex-

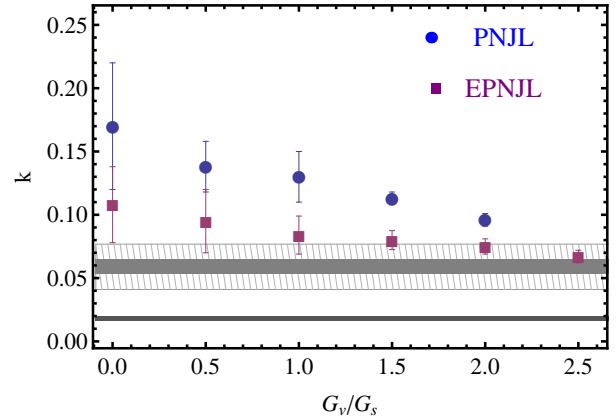


FIG. 9: Curvature  $k$  of the crossover line for the PNJL and EPNJL models as a function of  $G_v/G_s$ . The light-grey and grey bands are the (2+1)-flavor lattice QCD results from [31] and [34], respectively. The large shaded band corresponds to calculations with the imaginary chemical potential [33].

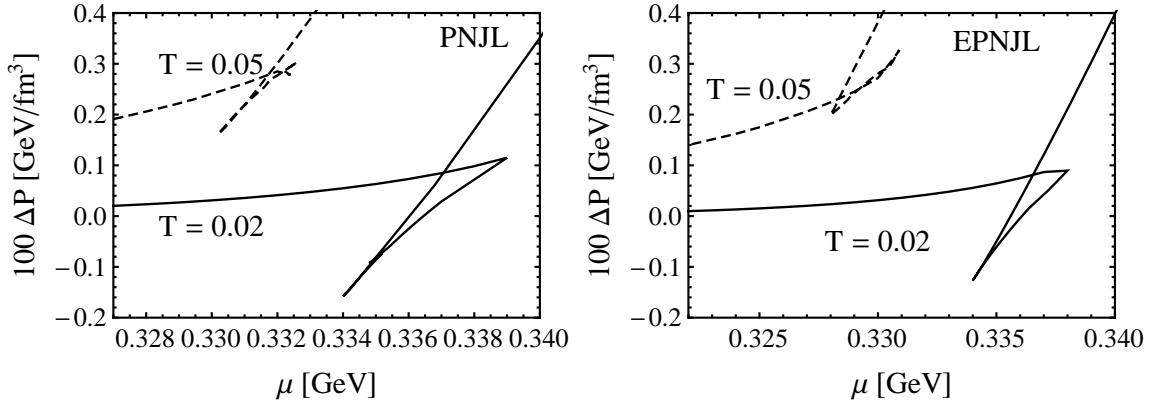


FIG. 10: Pressure quark chemical potential dependence at different temperatures in PNJL and EPNJL models.

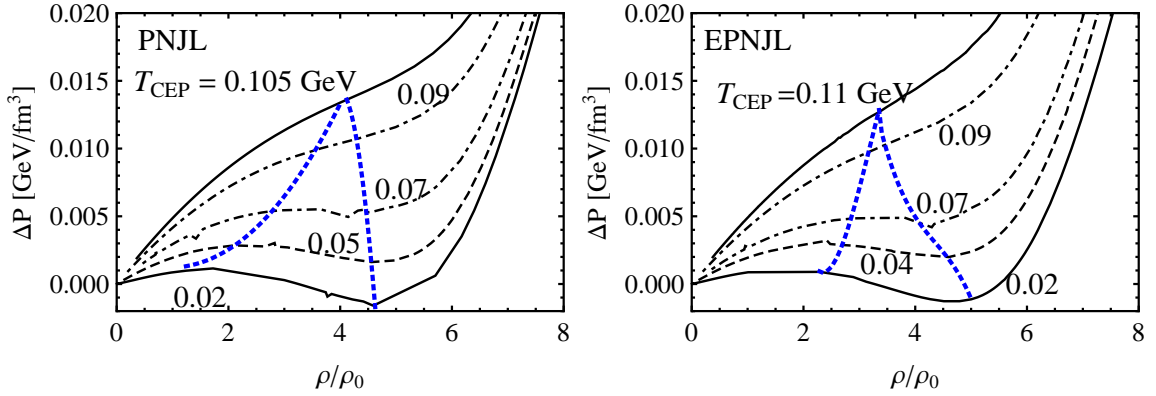


FIG. 11: Pressure-quark density dependence at different temperatures in the PNJL and EPNJL models. Dashed lines show the unstable spinodal boundaries.

pectation values computed at  $\mu = 0$ : by the Taylor expansion method, analytical continuation for small and real  $\mu_B$ , reweighting technique, determining the pseudo-critical line for purely imaginary values of  $\mu_B$  as discussed for example in Ref. [32]. According to the (2+1)-flavor lattice results for Taylor expansion technique [33],  $k = 0.059 \pm 0.020$  and also  $k = 0.0089 \pm 0.0014$  and  $k = 0.0066 \pm 0.0020$  deduced from the scaling properties of the chiral condensate and its susceptibility, respectively [31]. The (2+1)-flavor QCD results with the imaginary chemical potential  $k = 0.0132 \pm 0.0018$  obtained from the renormalized chiral condensate and renormalized chiral susceptibility  $k = 0.0132 \pm 0.003$  [32] seem to be compatible with those cited above and obtained from Taylor coefficients. In Fig. 9, the lattice measurements of the crossover line curvature  $k$  are plotted together with the PNJL and EPNJL model results as a function of  $G_v/G_s$ . The noted above shifting of the chiral crossover to larger  $\mu$  implies a flattening of the curvature of the crossover boundary in the neighborhood of  $\mu = 0$ . Standard NJL and PNJL calculations without vector interaction usually produce a curvature parameter  $k$  that is too large in comparison with the lattice results. Evidently, reasonably large vector coupling strength  $G_v/G_s \gtrsim 1$  is

capable of approaching such a small curvature in the case of EPNJL but not for PNJL.

The equation of state of quark matter is displayed in Figs. 10, 11. The mixed phase as coexistence of the hadronic and quark phases defined by the Maxwell construction manifests itself as a straight line connecting two branches in the triangle-loop formed near the critical point in the dependence of pressure on the chemical quark potential (Fig. 10). Two ends of this straight line correspond to the boundary of the coexisting phase. Assuming here the constant density within this range, one can define the isothermal sound velocity,

$$\nu_T^2 = \frac{\rho}{P_T + \epsilon} \left. \frac{\partial P}{\partial \rho} \right|_T.$$

These found numerically points (spinodals) limit a thermodynamically unstable spinodal phase region, where spinodal separation between confined and deconfined phases could occur. One should note that the spinodal region shrinks increasing  $G_v$ , i.e. at the fixed temperature the first-order phase transition gets weakened and eventually becomes the second order. This explains why the critical point moves to lower temperature and finally disappears from the phase diagram.

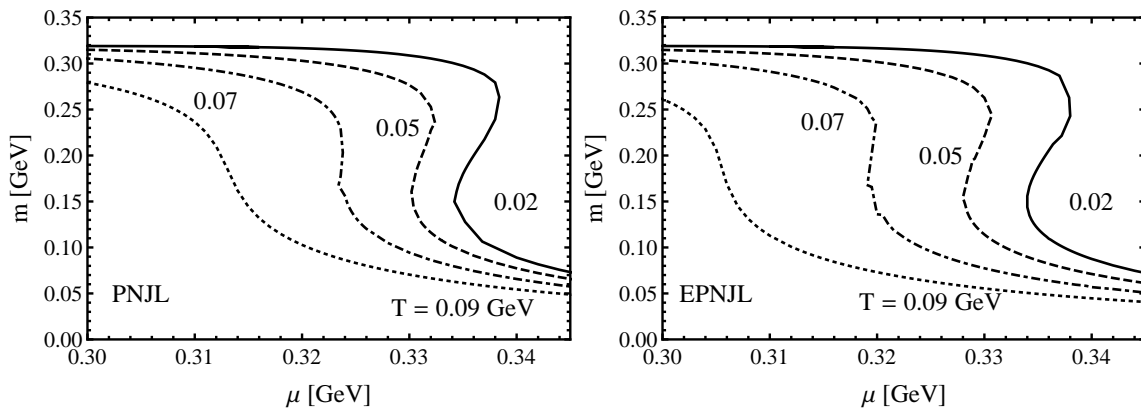


FIG. 12: Quark mass vs the quark chemical potential at different temperatures in PNJL and EPNJL models.

The spinodal region is shown in Fig. 11 by the dotted line as a function of the reduced density. One can define the boundaries of the unstable region also by the isentropic sound velocity

$$v_s^2 = \frac{\rho}{P_T + \epsilon} \left. \frac{\partial P}{\partial \rho} \right|_s$$

, but the high-temperature part of this region is smaller than that for isothermal spinodality and does not reach the critical end point [35].

As is seen from the comparison of Fig. 12 with Fig. 11, this instability range strongly correlates with the range where the quark mass derivative with respect to the chemical potential becomes negative,  $\partial m / \partial \mu < 0$ . Note that the location of the critical point ( $\sim 100$  MeV) is lower than that in lattice calculations.

## V. CONCLUDING REMARKS

The 2-flavor Polyakov-loop extended model is generalized by taking into account the effective four-quark vector interaction and its dependence on the Polyakov loop. The effective vertex generates entanglement interaction between the Polyakov loop and the chiral condensate. We investigated the impact of the entanglement interaction on thermodynamic properties of the system and, in particular, on the location of the critical end point at the given chemical potential or quark density. It is shown that these effects improve the model agreement with the lattice data.

The inclusion of the vector four-quark interaction shifts the location of the critical point towards lower temperature and larger chemical potential as compared to the standard NJL models. Additional account for entanglement between the deconfinement transition and the chiral symmetry restoration moves the critical end point in the opposite direction but it is not enough for the model to agree with the lattice result. While the exact value of the vector coupling strength is uncertain, our results clearly point to a strong vector repulsion

in the hadronic phase (large  $\mu$ ) and near-zero repulsion in the deconfined phase ( $\mu \rightarrow 0$ ) supporting conclusions of Ref. [30]. Our comparison between the lattice data and the PNJL/EPNJL results for the curvature of the crossover boundary supposes large values of  $G_v$ . At present, the vector coupling  $G_v$  cannot be determined from experiment and/or lattice QCD simulations but, eventually, the combination of neutron star observations and the energy scan of the phase-transition signals in the large  $\mu$  range at FAIR/NICA may provide us with some hints on its precise numerical value. While many authors consider  $G_v$  as a free parameter, whose values range in  $0.5 \leq G_v/G_s \leq 0.5$  [36, 37], other try to fix it in different ways as in Refs. [10, 20, 29, 38] predicting  $0.3 \leq G_v/G_s \leq 3.2$ , so that the true value remains undetermined.

It is possible that some new interaction should be added. In particular, the chiral phase transition in an extended Nambu-Jona-Lasinio model with scalar type eight-quark interactions is studied in [39]. The scalar type nonlinear term hastens the restoration of chiral symmetry, while the scalar-vector mixing term makes the transition sharper. The scalar type nonlinear term shifts the critical end point toward the values predicted by lattice QCD simulations and the QCD-like theory [9, 39]. Note that a sufficiently strong vector interaction is likely to provide the necessary repulsion at high density that helps supporting two-solar-mass neutron stars [40].

Our preliminary study shows that the discussed spinodal separation between the confined and deconfined phases in fact occurs in relativistic nuclear collisions and a more refined analysis is needed. To find signals of this spinodal separation is a challenge for future work.

## Acknowledgments

We are thankful to P. Costa and M. Ilgenfritz for useful discussions. This work has been supported in part by the LOEWE center HIC for FAIR as well as by BMBF and by the RFBR, grant No. 13-01-00060a (Yu.L.K). V.D.T. is also partly supported by the Russian Ministry of Science and Education, research project identifier RFMEFI61614X0023 and by the Heisenberg-Landau



grant of JINR.

- 
- [1] K. Fukushima, Phys. Lett. **B591**, 277 (2004).  
 [2] C. Ratti, M. A. Thaler, W. Weise, Phys. Rev. **D73**, 014019 (2006).  
 [3] Y. Sakai, T. Sasaki, H. Kouno, M. Yahiro, Phys. Rev. **D82**, 076003 (2010).  
 [4] Y. Sakai, T. Sasaki, H. Kouno, M. Yahiro, Phys. Rev. **D84**, 091901 (2011).  
 [5] Y. Sakai *et al.*, Phys. Rev. **D78**, 076007 (2008).  
 [6] U. Wogl, W. Weise, Prog. Part. Nucl. Phys. **27**, 195 (1994).  
 [7] T. Hatsuda, T. Kunihiro, Phys. Rep. **247**, 221 (1994).  
 [8] M. Bubbala, Phys. Rep. **407**, 205 (2005).  
 [9] K. Kashiwa, T. Hell and W. Weise, Phys. Rev. **D84**, 096001 (2009).  
 [10] M. Dutra, O. Loureno, A. Delfino, T. Frederico, M. Malheiro, Phys. Rev. **D88**, 114013 (2013).  
 [11] H. Hansen *et al.*, Phys. Rev. **D75**, 065004 (2007).  
 [12] M. Cheng *et al.*, Phys. Rev. **D77** 014511 (2008).  
 [13] S. Borsanyi *et al.*, arXiv:1005.3508.  
 [14] A. Bazanov and P. Petreczky, PoS Latt 2009 (2009) 163; arXiv1005.1131  
 [15] P. de Forcrand and O. Philipsen, Nucl. Phys. **B642**, 290 (2002)  
 [16] M. D’Elia and M. P. Lombardo, Phys. Rev. **D67**, 014505 (2003).  
 [17] M. D’Elia and M. P. Lombardo, Phys. Rev. **D70**, 074509 (2004).  
 [18] H. S. Chen and X. Q. Luo, Phys. Rev. **D72**, 034504 (2005).  
 [19] L. K. Wu, X. Q. Luo, H. S. Chen, Phys. Rev. **D76**, 034505 (2007).  
 [20] Y. Sakai *et al.*, Phys. Rev. **D79**, 096001 (2009).  
 [21] Y. Sakai, T. Sasaki, H. Kuono, and M. Yahiro, J. Phys. **G39**, 035004 (2012).  
 [22] M. C. Ruivo, P. Costa, C. A. de Suosa, Phys. Rev. **D86**, 116007 (2012).  
 [23] J. Sugano *et al.*, Phys. Rev. **D90**, 037901 (2014).  
 [24] T. Kähärä and K. Tuominen, Phys. Rev. **D78**, 034015 (2008).  
 [25] A. Ali Khan *et al.*, Phys. Rev. **D64**, 074510 (2001).  
 [26] C.R. Allton, S. Ejiri, S.J. Hands *et al.*, Phys. Rev. **D68**, 014507 (2003).  
 [27] M. Kaczmarek and F. Zantov, Phys. Rev. **D71**, 114510 (2005).  
 [28] J.D. Kogut and D.K. Sinclair, Phys. Rev. **D70**, 094501 (2004).  
 [29] K. Kashiwa, T. Hell and W. Weise, Phys. Rev. **D71**, 056010 (2011).  
 [30] J. Steinheimer and S. Schramm, Phys. Lett. **B736**, 241 (2014).  
 [31] G. Endrodi, Z. Fodor, S.D. Katz and K.K. Szabo, JHEP **1104**, 001 (2011).  
 [32] C. Bonati, M. D’Elia, M. Mariti, M. Mesiti, F. Negro and F. Sanfilippo, arXiv:1410.5758.  
 [33] O. Kaczmarek, F. Karsch *et al.*, Phys. Rev. **D83**, 014504 (2011).  
 [34] P. Cea, L. Cosmai, and A. Papa, Phys. Rev. **D89**, 074512 (2014).  
 [35] J. Randrup, Nucl. Phys. **A752**, 384c (2005); Phys. Rev. **C82**, 34902 (2010).  
 [36] R. Rapp, T. Schaffer, E.V. Shuryak and M. Velkovski, Phys. Rev. Lett. **D82**, 53 (1998).  
 [37] S. Carignano, D. Nickel and M. Bubbala, Phys. Rev. **D85**, 0540009 (2010).  
 [38] N.M. Bratovic, T. Hatsuda and W. Weise, Phys. Lett. **B719**, 131 (2013).  
 [39] K. Kashiwa, H. Kouno, T. Sakaguchi, M. Matsuzaki and M. Yahiro, Phys. Lett. **B647**, 446 (2007).  
 [40] F. Ozel, G. Baym, and T. Guver, Phys.Rev. **D82**, 101301 (2010).